Theoretical Study on Triplet Potential Energy Surface of the $CH(^2\Pi) + NO_2$ Reaction

Yu-guo Tao,* Yi-hong Ding, Ze-sheng Li, Xu-ri Huang, and Chia-Chung Sun

State Key Laboratory of Theoretical and Computational Chemistry, Institute of Theoretical Chemistry, Jilin University, Changchun 130023, People's Republic of China

Received: June 29, 2001; In Final Form: August 20, 2001

A detailed theoretical survey on the triplet potential energy surface (PES) for the CH + NO_2 reaction is carried out at the B3LYP and CCSD(T) (single-point) levels in order to gain a deeper mechanistic knowledge of this important radical reaction. Thirty-eight minimum isomers and 107 transition states are located. It is shown that the CH and NO_2 radicals can be brought together barrierlessly via the triplet PES to form the initial N-attack adduct $HCNO_2$ (**1**) that lies 50.6 kcal/mol below the reactant **R**. Subsequently, the most feasible channel is the direct O-extrusion of **1** to produce $\mathbf{P_6}$ (HCNO + ^{3}O) with the barrier 31.2 kcal/mol. The less competitive channel is a 1,3-H shift conversion of **1** to the branched isomer HON(O)C (**10**) (34.2 kcal/mol below **R**) with a barrier 37.1 kcal/mol, which can directly dissociate to product $\mathbf{P_9}$ (CNO + OH) with a small barrier 9.0 kcal/mol. However, the oxygen-shift conversion of **1** leading to the very low lying isomers OC(H)NO (**2**) (**2′**) that can directly dissociate to $\mathbf{P_1}$ (HCO + NO) and then $\mathbf{P_{12}}$ (H + CO + NO) needs a much larger barrier, 43.3 kcal/mol. This is in sharp contrast to the mechanism of the title reaction via the singlet PES (Tao; et al. *J. Phys. Chem. A* **2001**, *105*, 3388) that the exclusive feasible channel proceeds via the almost barrierless oxygen-shift conversion of $HCNO_2$ to OC(H)NO followed by formation of HCO + NO (major), HNO + CO, and HON + CO (minor), each of which can take secondary dissociation to the final product H + CO + NO. Since all appropriate transition states and intermediates lie below **R**, the overall rate constant of the title reaction via the triplet PES is expected to be fast, as confirmed by the simple RRKM calculations ($k_{298K} = 5.14 \times 10^{-12}$ cm^{3}molecule^{-1} s^{-1}). Since the predicted products of the title reaction via the triplet PES is completely different from that via the singlet PES, we feel that future experimental investigations on this radical reaction are desirable.

1. Introduction

The radical reaction of CH with NO_2 plays an important role in combustion processes, which are related to the prompt NO-formation and NO-reburning mechansim.[1] The total rate constant of this reaction was measured to be $k = 1.67 \pm 0.11 \times 10^{-10}$ cm^3 molecule^{-1} s^{-1} at 298 K by Wagal et al.[2] in 1982. Recently, in 1998, Rim and Hershberger[3] reported the direct measurements of the product branching ratios at 296 K using multiphoton photolysis of $CHBr_3$ at 248 nm followed by time-resolved infrared diode laser products detection. On the basis of consideration of product yields and secondary chemistry, they found that the major product channel is H + CO + NO or HNO + CO, which together account for 92 ± 4% of the total rate constant, whereas the minor product channel is HCO + NO, accounting for 8 ± 4%.

Very recently, Tao et al.[4] performed a detailed theoretical investigation on the singlet potential energy surface of the title reaction. The initial step is the side attack of the CH radical on NO π bonding of NO_2 to form isomer $HCNO_2$ that can convert almost with no barrier to the very low lying isomers OC(H)-NO followed by direct dissociation to product HCO + NO. Much less competitively, OC(H)NO can either dissociate to product HNO + CO or isomerize to a weakly bound complex HON···CO that dissociates very easily to product HON + CO. The large reaction heat released from the reactant may make most of the products HCO + NO, HNO + CO, and HON + CO to take further dissociation to the final product H + CO + NO. Yet observation of the other products seems unlikely due to either thermodynamical or kinetic hindrance. Their calculated results on singlet PES of the title reaction are in excellent agreement with Rim and Hershberger's experiment.[3]

Principally, two doublet radicals can be brought together either via a singlet or a triplet PES. A typical example is the CH + NO reaction, which has been considered as a key process for modeling nitrogen chemistry in flames and has been the subject of numerous theoretical and experimental investigations.[5] Particularly, in a series of theoretical work, Rayez et al.[6] have shown that the triplet PES may play a major role in the reaction of CH + NO with respect to the singlet PES (they found that the singlet PES has a slight entrance barrier of 1.2 kcal/mol whereas the triplet one is barrierless). Their results were consistent with available experimental findings.[7] Then, for the title CH + NO_2 reaction, it is very reasonable for us to suggest that the triplet PES may also play a part though the singlet PES calculated by Tao et al.[4] is barrierless and can well interpret Rim and Hershberger's experiment.[3] Moreover, a detailed study on the triplet PES of $CHNO_2$ is desirable at least from a theoretical viewpoint to explore why some very low lying triplet products such as ^{3}NH + CO_2, HCN + $^3O_2$ and HNCO + ^{3}O (they are more associated with the triplet PES than with the singlet PES) were not observed in previous experiment.[2,3] A comprehensive knowledge about the PES in both singlet and triplet states of the CH + NO_2 reaction may help us gain a deeper understanding of the N-containing combustion chemistry.

10.1021/jp012481u CCC: $20.00
Published on Web 09/15/2001

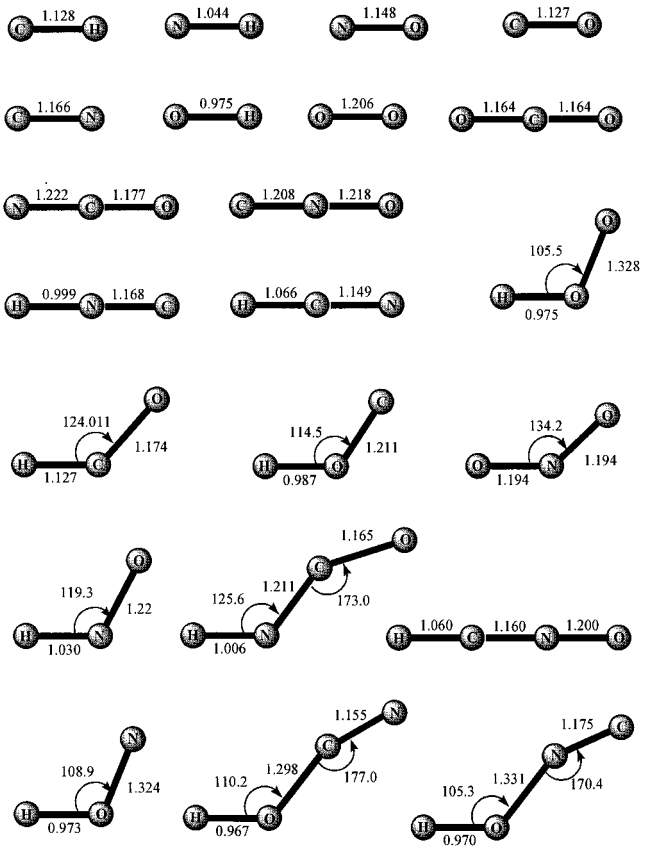

Figure 1. B3LYP/6-311G(d,p) optimized geometries for reactant and products. Bond lengths are in angstroms and angles in degrees.

In fact, the present study reveals that the CH and NO_2 radicals can proceed barrierlessly via the triplet PES of $CHNO_2$ to form the initial N-attack adduct $CHNO_2$. A notable finding is that $CHNO_2$ can more favorably dissociate to product HCNO + ^{3}O and CNO + OH than to HCO + NO and H + CO + NO. Discussions are made on the discrepancies between the singlet and triplet PES of $CHNO_2$ and on implications of the possible role of the triplet PES.

2. Computational Methods

All computations are carried out using the GAUSSIAN98 program package.[8] The optimized geometries and harmonic frequencies of the reactant, products, local minima, and transition states structures are obtained at the B3LYP/6-311G(d,p) level. Moreover, single-point calculations are performed at the CCSD(T)/6-311G(d,p) level using the B3LYP/6-311G(d,p) optimized geometries. The zero-point vibration energy (ZPVE) at the B3LYP/6-311G(d,p) level is also included. To confirm whether the obtained transition states connect with the right reactants and products, the intrinsic reaction coordinate (IRC) calculations are performed at the B3LYP/6-311G(d,p) level.

3. Results and Discussion

Starting from the reactant **R** ($CH + NO_2$), 19 products (**P_1**−**P_{19}**) related to the triplet PES are considered. Their structures are depicted in Figure 1, and total and relative energies are listed in Table 1. The structures of 38 intermediate $CHNO_2$ isomers in triplet are shown in Figure 2 with their corresponding energies in Table 2. A total of 107 interconversion transition states are located connecting various isomers or products. The structures of the transition states are described in Figure 3 and energies listed in Table 3. The potential curves of the initial N-attack of the CH radical to NO_2 are presented in Figure 4. The reaction pathways of the $CH + NO_2$ reaction via the triplet PES are schematically plotted in Figure 5.

3.1. Initial Attack. We consider three possible initial attack sites of CH at NO_2, i.e., top-N attack, end-O attack, and side-NO π bonding attack. The top-N attack can barrierlessly lead to the triplet adduct isomer $HCNO_2$ (**1**), as confirmed by the calculated pointwise potential curves at both the B3LYP/6-311G(d,p) (in Figure 4a) and CCSD(T)/6-311G(d,p) (in Figure 4b) levels. In isomer **1**, the two N−O bonds are very similar (1.239 and 1.227 Å) and are slightly longer than that (1.194 Å) in NO_2. We cannot locate either the isomer or the transition state associated with the end-O attack. Searching for such a triplet end-O attack isomer usually leads to the separate species HCO and NO. We expect that the direct O-abstraction from NO_2 is a barrier-consumed process in view of the strong N−O bonding. Also, optimization of the side-NO π bonding attack isomer often leads to the top-N attack species **1**. Therefore, on the triplet PES of the $CH + NO_2$ reaction, the exclusive feasible entrance channel is the barrierless top-N attack of CH at NO_2 to form $HCNO_2$ (**1**). The barrierless nature for the entrance

TABLE 1: Total (au) and Relative Energies in Parentheses (kcal/mol) as Well as Those Including Zero-Point Vibration Energies (kcal/mol) of the Reactant and Products for the $CH + NO_2$ Reaction

species	B3LYP/6-311G**	CCSD(T)/6-311G**	CCSD(T)/6-311G**+ZPVE
R ($CH + NO_2$)	−243.6246931/(0.0)	−243.0625676/(0.0)	0.0
P_1 (HCO + NO)	−243.8132973/(−118.4)	−243.2556415/(−121.2)	−119.7
P_2 (^{3}HNO + CO)	−243.8392494/(−134.6)	−243.2802440/(−136.6)	−134.5
P_3 (^{3}HON + CO)	−243.8230922/(−124.5)	−243.2717966/(−131.3)	−129.1
P_4 (^{3}NH + CO_2)	−243.8781971/(−159.1)	−243.3232097/(−163.6)	−161.1
P_5 (HNCO + ^{3}O)	−243.8183517/(−121.5)	−243.2607273/(−124.3)	−120.4
P_6 (HCNO + ^{3}O)	−243.7079889/(−52.3)	−243.1478365/(−53.5)	−50.5
P_7 (HCN + $^3O_2$)	−243.8168088/(−120.6)	−243.2578818/(−122.3)	−119.1
P_8 (NCO + OH)	−243.8045307/(−112.8)	−243.2408336/(−111.9)	−109.8
P_9 (CNO + OH)	−243.7037902/(−49.6)	−243.1402343/(−48.7)	−47.4
P_{10} (CN + HO_2)	−243.6872754/(−39.3)	−243.1306622/(−42.7)	−40.3
P_{11} (HNC + $^3O_2$)	−243.7931798/(−105.7)	−243.2329897/(−106.9)	−104.2
P_{12} (HOC + NO)	−243.7463111/(−76.3)	−243.1899551/(−79.9)	−78.4
P_{13} (HONC + ^{3}O)	−243.6785225/(−33.8)	−243.1297331/(−42.1)	−39.0
P_{14} (HOCN + ^{3}O)	−243.7728657/(−93.0)	−243.2236386/(−101.1)	−97.1
P_{15} (H + CO + NO)	−243.7750935/(−94.4)	−243.2336925/(−107.4)	−110.9
P_{16} (H + ^{3}O + CNO)	−243.5368043/(55.2)	−242.9847450/(48.8)	44.8
P_{17} (H + ^{3}O + NCO)	−243.6375448/(−8.1)	−243.0854738/(−14.4)	−17.6
P_{18} (OH + CN + ^{3}O)	−243.5767806/(30.1)	−243.0387470/(14.9)	13.8
P_{19} (H + CN + $^3O_2$)	−243.6038144/(13.1)	−243.0532984/(5.8)	1.7

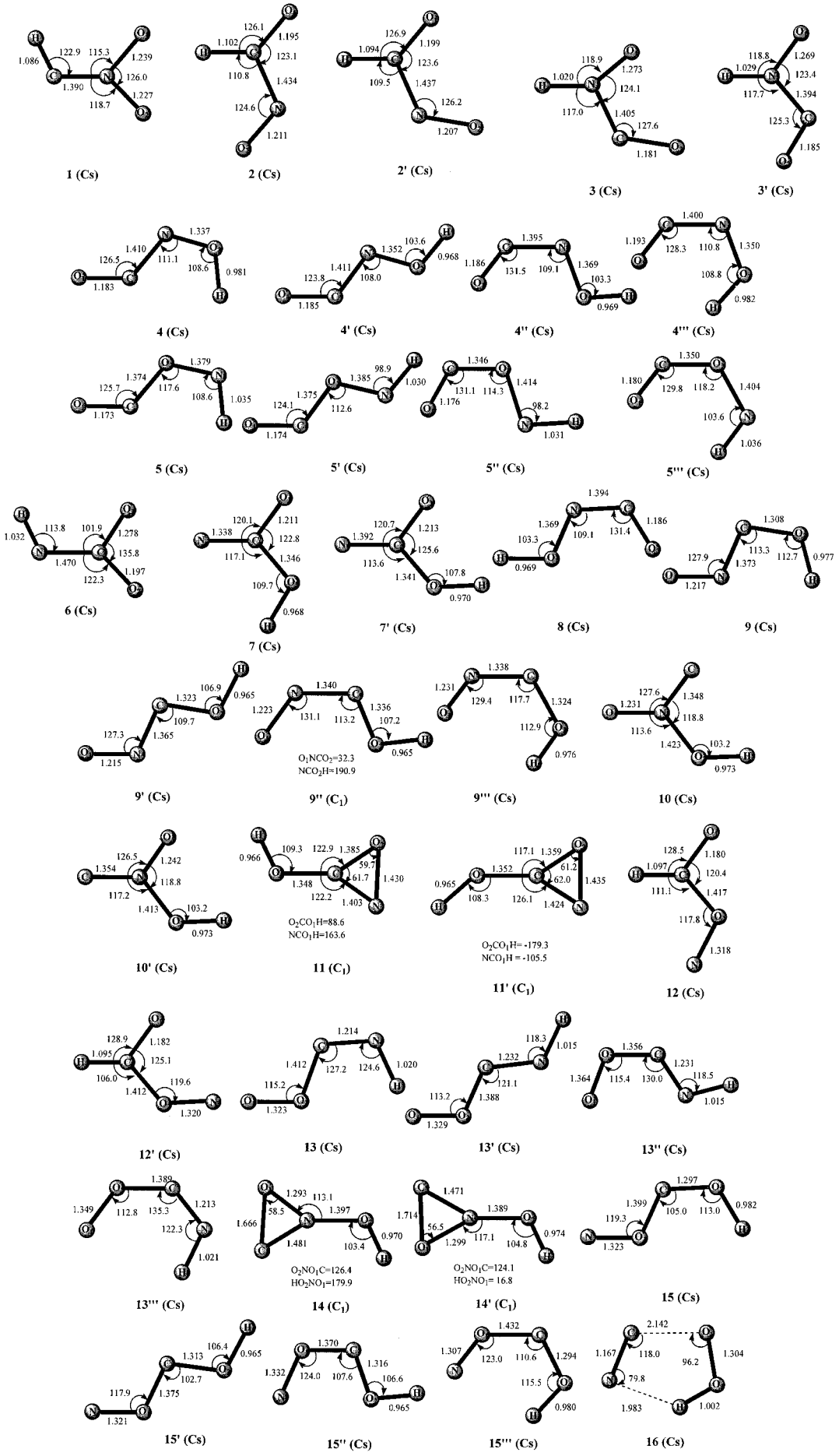

Figure 2. B3LYP/6-311G(d,p) optimized geometries for $CHNO_2$ isomers at triplet. Bond lengths are in angstroms and angles in degrees.

TABLE 2: Total (au) and Relative Energies in Parentheses (kcal/mol) as Well as Those Including Zero-Point Vibration Energies (kcal/mol) of the Isomers for the $CH + NO_2$ Reaction at Triplet

species	B3LYP/6-311G**	CCSD(T)/6-311G**	CCSD(T)/6-311G**+ZPVE
1	−243.7215823/(−60.8)	−243.1512700/(−55.7)	−50.6
2	−243.8573537/(−146.0)	−243.2824047/(−137.9)	−132.0
2'	−243.8583588/(−146.6)	−243.2833746/(−138.6)	−132.3
3	−243.8328402/(−130.6)	−243.2582942/(−122.8)	−116.4
3'	−243.8327360/(−130.5)	−243.2576812/(−122.4)	−116.3
4	−243.8185911/(−121.7)	−243.2478045/(−116.2)	−110.5
4'	−243.8198282/(−122.4)	−243.2500080/(−117.6)	−116.6
4''	−243.8135802/(−118.5)	−243.2439852/(−113.8)	−108.0
4'''	−243.8129664/(−118.1)	−243.2433406/(−113.4)	−107.5
5	−243.8034020/(−112.1)	−243.2350073/(−108.2)	−103.1
5'	−243.8074406/(−114.7)	−243.2395764/(−111.1)	−105.7
5''	−243.8056560/(−113.6)	−243.2380010/(−110.1)	−104.8
5'''	−243.8037004/(−112.3)	−243.2358238/(−108.7)	−103.5
6	−243.8474713/(−139.8)	−243.2734847/(−132.4)	−127.6
7	−243.8645915/(−153.1)	−243.3005381/(−149.3)	−143.2
7'	−243.8686791/(−153.1)	−243.3059411/(−152.7)	−146.4
8	−243.8135803/(−118.5)	−243.2439697/(−113.8)	−107.9
9	−243.7999155/(−110.0)	−243.2244970/(−101.6)	−96.0
9'	−243.8018342/(−111.2)	−243.2269152/(−103.1)	−97.1
9''	−243.7851293/(−100.7)	−243.2099131/(−92.9)	−87.0
9'''	−243.7803425/(−97.7)	−243.2043881/(−89.0)	−84.0
10	−243.6978223/(−45.9)	−243.1251871/(−39.3)	−34.2
10'	−243.6968862/(−45.3)	−243.1242835/(−38.7)	−33.7
11	−243.7701906/(−91.3)	−243.2051822/(−89.5)	−83.9
11'	−243.7708871/(−91.7)	−243.2058748/(−89.9)	−84.6
12	−243.8316714/(−129.9)	−243.2665289/(−128.0)	−122.5
12'	−243.8332514/(−130.9)	−243.2633526/(−129.2)	−123.6
13	−243.7355003/(−69.5)	−243.1603492/(−61.4)	−57.1
13'	−243.7437587/(−74.7)	−243.1699691/(−67.4)	−62.5
13''	−243.7428332/(−74.1)	−243.1691416/(−66.9)	−62.0
13'''	−243.7363872/(−70.1)	−243.1624670/(−62.7)	−58.2
14	−243.6519678/(−17.1)	−243.0829794/(−12.8)	−8.7
14'	−243.6532530/(−17.9)	−243.0842222/(−13.6)	−9.3
15	−243.7623067/(−86.4)	−243.2012536/(−87.0)	−82.1
15'	−243.7643009/(−87.6)	−243.2029537/(−88.1)	−82.7
15''	−243.7623418/(−86.4)	−243.2006903/(−86.7)	−81.4
15'''	−243.7569098/(−83.0)	−243.1936655/(−82.3)	−77.7
16	−243.7106354/(−53.9)	−243.1406638/(−49.0)	−44.6

channel is similar to the singlet PES.[4] A slight difference is that on the singlet PES, CH and NO_2 react to form the side-NO π bonding attack isomer $HCNO_2$ with one N−O significantly elongated (1.307 Å) and the other hardly changed (1.191 Å) with respect to that (1.194 Å) in NO_2. This can be rationalized that on the singlet PES, CH both behaves a radical and a carbene character while on the triplet PES, the radical character predominates.

3.2. Isomerization and Dissociation. For the $CH + NO_2$ reaction, the triplet PES is very complex. Parts a−c of Figure 5 schematically show various isomerization and dissociation pathways. From Figure 5a, we can see that the initially formed adduct $HCNO_2$ (**1**) may take many conversion pathways such as

Path $\mathbf{P_6}$: $\mathbf{R \rightarrow 1 \rightarrow P_6}$ (HCNO + ^{3}O)

Path $\mathbf{P_9}$: $\mathbf{R \rightarrow 1 \rightarrow 10 \rightarrow P_9}$ (CNO + OH)

Path $\mathbf{P_{13}}$: $\mathbf{R \rightarrow 1 \rightarrow 10 \rightarrow P_{13}}$ (HONC+^{3}O)

Path $\mathbf{P_3}$: $\mathbf{R \rightarrow 1 \rightarrow 10}$, $\mathbf{10' \rightarrow 14}$, $\mathbf{14' \rightarrow P_3}$ (^{3}HON + CO)

Path $\mathbf{P_2}$, $\mathbf{P_{12}}$, $\mathbf{P_{14}}$: $\mathbf{R \rightarrow 1 \rightarrow 10 \rightarrow 9}$, $\mathbf{9'}$, $\mathbf{9''}$, $\mathbf{9'''} \rightarrow$ $\mathbf{P_2}$ (^{3}HNO + CO), $\mathbf{P_{12}}$ (HOC + NO), $\mathbf{P_{14}}$ (HOCN + ^{3}O)

Path $\mathbf{P_1}$: $\mathbf{R \rightarrow 1 \rightarrow 2}$, $\mathbf{2' \rightarrow P_1}$ (HCO + NO)

By considering the conversion barrier heights and the relative energies of the transition states involved in these pathways, we can deduce the most feasible one starting from the reactant **R**.

The easiest and also the simplest pathway is surely path $\mathbf{P_6}$ that proceeds via the direct dissociation to $\mathbf{P_6}$ (HCNO + ^{3}O) via an O-extrusion transition state **TS1/P$_6$** with a barrier 31.2 kcal/mol. The less feasible pathways are path**s** $\mathbf{P_9}$ and $\mathbf{P_{13}}$, which proceed first via a 1,3-H shift of **1** to the branched isomer HON(O)C (**10**) with a barrier of 37.1 kcal/mol followed by direct N−O cleavage either to product $\mathbf{P_9}$ (CNO + OH) or to $\mathbf{P_{13}}$ (HONC + ^{3}O). Since the barrier 9.0 kcal/mol for $\mathbf{10 \rightarrow P_6}$ conversion is significantly lower than 22.4 kcal/mol for $\mathbf{10 \rightarrow P_{13}}$, $\mathbf{P_6}$ is certainly the second feasible pathway.

In path $\mathbf{P_3}$, the conversion from **10** to its isomeric form **10′** takes place very easily. **10** (**10′**) may proceed via a ring-closure process to form the isomer HO−cNCO (**14** (**14′**)) that can dissociate directly to the very-lying products $\mathbf{P_3}$ (^{3}HON + CO). In path $\mathbf{P_2}$, $\mathbf{P_{12}}$, $\mathbf{P_{14}}$, the intermediate **10** can isomerize to the chainlike species HOCNO (**9′**) via a −OH group migration. **9′** can interconvert to its isomeric forms **9**, **9″**, and **9‴**. These HOCNO species can either take a direct N−O and C−N rupture to give $\mathbf{P_{14}}$ (HOCN + ^{3}O) and $\mathbf{P_{12}}$ (HOC + NO), respectively, or take a concerted 1,3-H shift and C−N cleavage to give the low-lying $\mathbf{P_2}$ (^{3}HNO + CO). However, we can also find that the rate-determining transition states **TS10/14** (−6.2), **TS10′/**

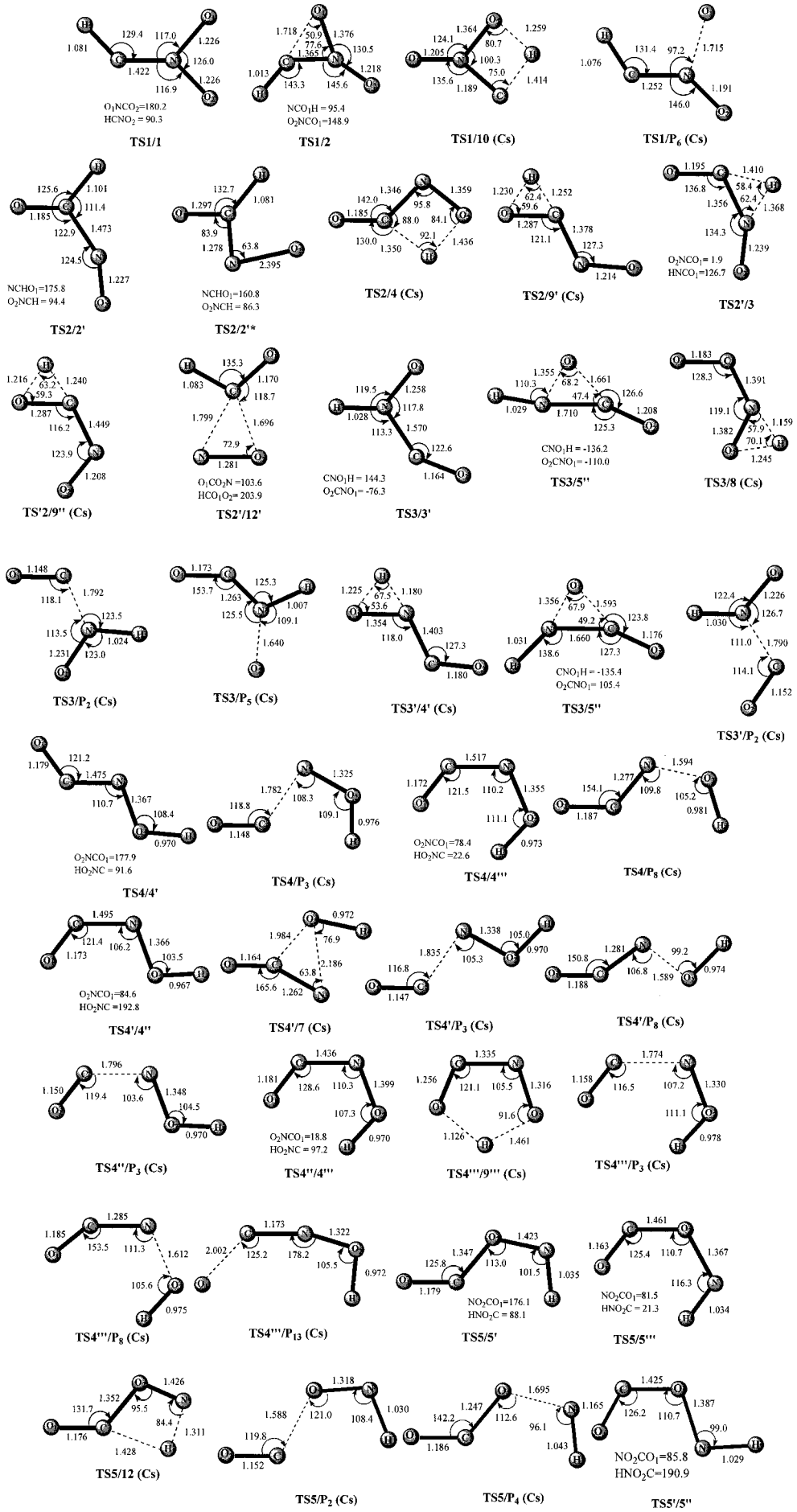
TS1/1
TS1/2
TS1/10 (Cs)
TS1/P6 (Cs)
TS2/2'
TS2/2'*
TS2/4 (Cs)
TS2/9' (Cs)
TS2'/3
TS'2/9'' (Cs)
TS2'/12'
TS3/3'
TS3/5''
TS3/8 (Cs)
TS3/P2 (Cs)
TS3/P5 (Cs)
TS3'/4' (Cs)
TS3/5''
TS3'/P2 (Cs)
TS4/4'
TS4/P3 (Cs)
TS4/4'''
TS4/P8 (Cs)
TS4'/4''
TS4'/7 (Cs)
TS4'/P3 (Cs)
TS4'/P8 (Cs)
TS4''/P3 (Cs)
TS4''/4'''
TS4'''/9''' (Cs)
TS4'''/P3 (Cs)
TS4'''/P8 (Cs)
TS4'''/P13 (Cs)
TS5/5'
TS5/5'''
TS5/12 (Cs)
TS5/P2 (Cs)
TS5/P4 (Cs)
TS5'/5''

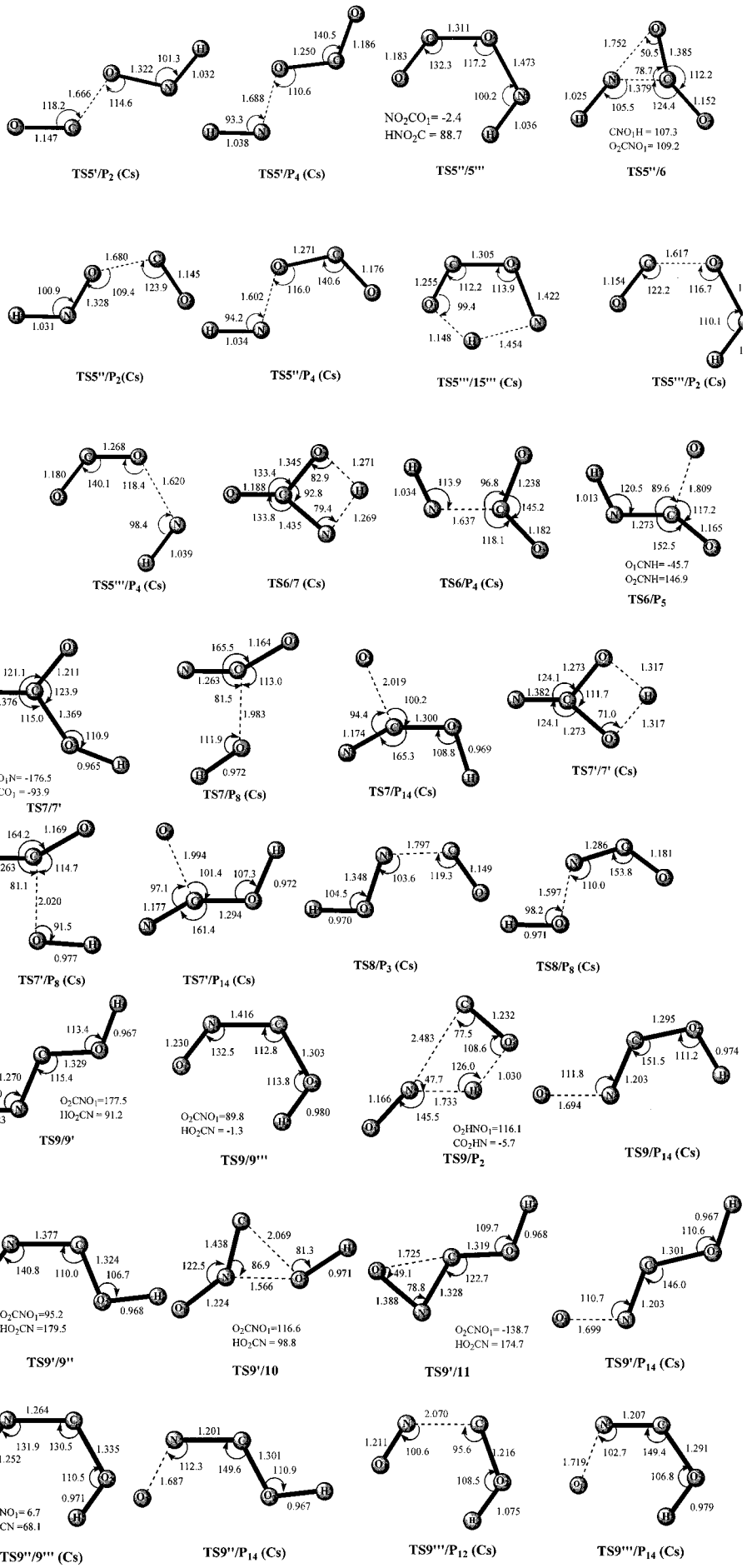
TS5'/P2 (Cs)
TS5'/P4 (Cs)
TS5''/5'''
NO2CO1= -2.4
HNO2C = 88.7
TS5''/6
CNO1H = 107.3
O2CNO1= 109.2
TS5''/P2(Cs)
TS5''/P4 (Cs)
TS5'''/15''' (Cs)
TS5'''/P2 (Cs)
TS5'''/P4 (Cs)
TS6/7 (Cs)
TS6/P4 (Cs)
O1CNH= -45.7
O2CNH=146.9
TS6/P5
O2CO1N= -176.5
HO2CO1 = -93.9
TS7/7'
TS7/P8 (Cs)
TS7/P14 (Cs)
TS7'/7' (Cs)
TS7'/P8 (Cs)
TS7'/P14 (Cs)
TS8/P3 (Cs)
TS8/P8 (Cs)
O2CNO1=177.5
HO2CN = 91.2
TS9/9'
O2CNO1=89.8
HO2CN = -1.3
TS9/9'''
O2HNO1=116.1
CO2HN = -5.7
TS9/P2
TS9/P14 (Cs)
O2CNO1=95.2
HO2CN =179.5
TS9'/9''
O2CNO1=116.6
HO2CN = 98.8
TS9'/10
O2CNO1= -138.7
HO2CN = 174.7
TS9'/11
TS9'/P14 (Cs)
O2CNO1= 6.7
HO2CN =68.1
TS9''/9''' (Cs)
TS9''/P14 (Cs)
TS9'''/P12 (Cs)
TS9'''/P14 (Cs)

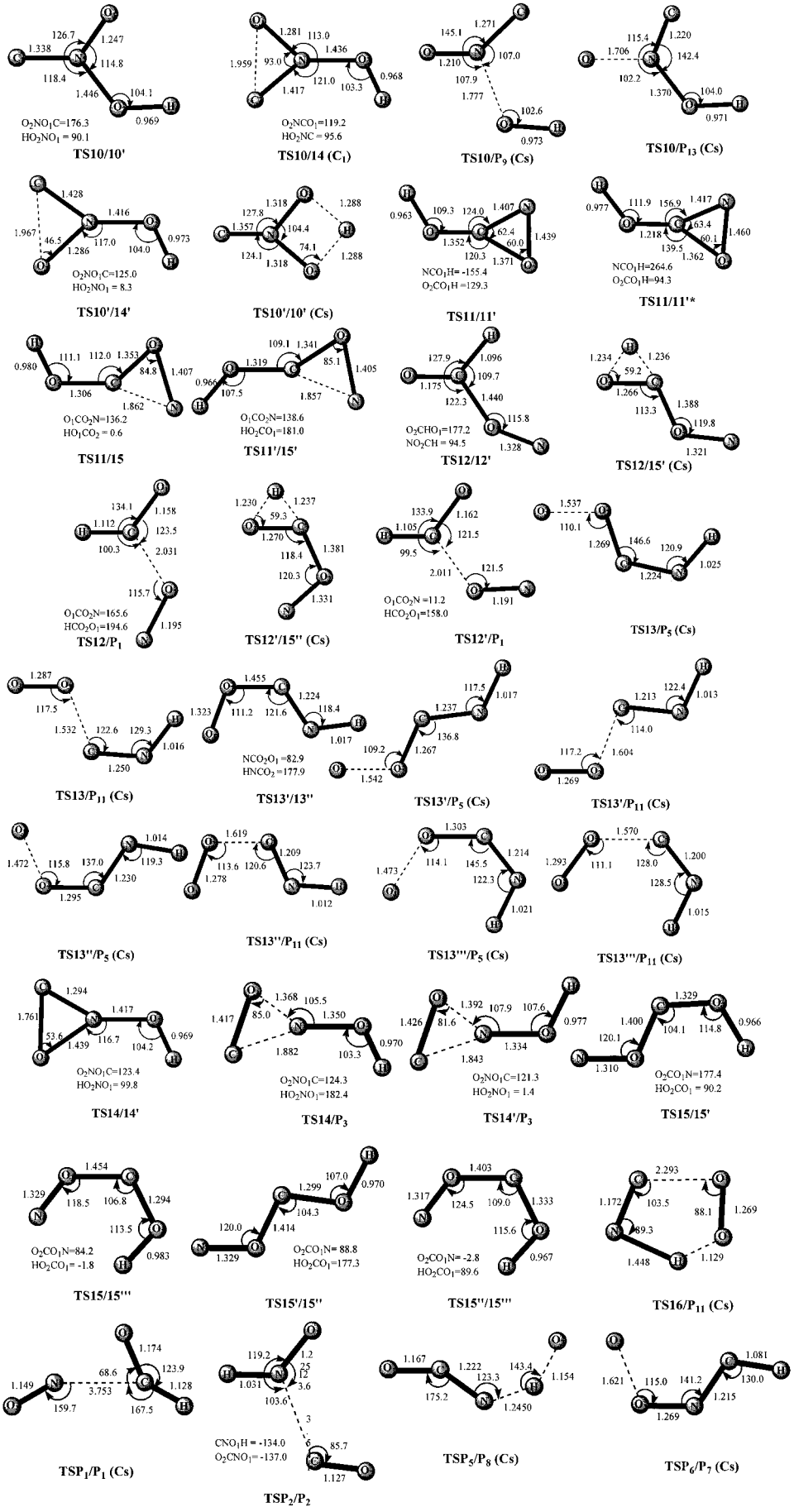

Figure 3. B3LYP/6-311G(d,p) optimized geometries for $CHNO_2$ transition states at triplet. Bond lengths are in angstroms and angles in degrees.

TABLE 3: Total (au) and Relative Energies in Parentheses (kcal/mol) as Well as Those Including Zero-Point Vibration Energies (kcal/mol) of the Transition States for the $CH + NO_2$ Reaction at Triplet

species	B3LYP/6-311G**	CCSD(T)/6-311G**	CCSD(T)/6-311G**+ZPVE
TS1/1	−243.7090453/(−52.9)	−243.1424937/(−50.2)	−45.7
TS1/2	−243.6577779/(−20.8)	−243.0801594/(−11.0)	−7.3
TS1/10	−243.6631141/(−24.1)	−243.0882062/(−16.1)	−13.5
TS1/P6	−243.6789333/(−34.0)	−243.0991297/(−22.9)	−19.4
TS2/2′	−243.8397519/(−135.0)	−243.2677423/(−128.7)	−123.3
TS2/2′*	−243.6736064/(−30.7)	−243.1127913/(−31.5)	−28.2
TS2/4	−243.7694499/(−90.8)	−243.1933764/(−82.1)	−79.7
TS2/9′	−243.7413009/(−73.2)	−243.1629837/(−63.0)	−60.9
TS2′/3	−243.7468962/(−76.7)	−243.1669414/(−65.5)	−63.5
TS2′/9″	−243.7247997/(−62.8)	−243.1509881/ (−55.5)	−54.0
TS2′/12′	−243.7956721/(−107.3)	−243.2265121/(−102.9)	−98.4
TS3/3′	−243.8102072/(−116.4)	−243.2372045/(−109.6)	−105.1
TS3/5″	−243.7575208/(−83.4)	−243.1865514/(−77.8)	−73.6
TS3/8	−243.7377537/(−70.9)	−243.1650292/(−64.3)	−62.6
TS3/P2	−243.8199541/(−122.5)	−243.2463761/(−115.3)	−111.3
TS3/P5	−243.7953637/(−107.1)	−243.2172945/(−97.1)	−92.6
TS3′/4′	−243.7440871/(−74.9)	−243.1700965/(−67.5)	−65.8
TS3′/5″	−243.7590138/(−84.3)	−243.1873284/(−78.3)	−74.1
TS3′/P2	−243.8177962/(−121.2)	−243.2436081/(−113.6)	−109.9
TS4/4′	−243.7936778/(−106.0)	−243.2252854/(−102.1)	−98.1
TS4/P3	−243.8089017/(−115.6)	−243.2433268/(−113.5)	−109.4
TS4/4‴	−243.7970200/(−108.1)	−243.2295204/(−104.8)	−100.3
TS4/P8	−243.7850549/(−100.6)	−243.2033162/(−88.3)	−84.2
TS4′/4″	−243.8028357/(−111.8)	−243.2360761/(−108.9)	−103.9
TS4′/7	−243.8112657/(−117.1)	−243.2338209/(−107.5)	−103.5
TS4′/P3	−243.8069303/(−114.4)	−243.2425067/(−112.9)	−108.9
TS4′/P8	−243.7899749/(−103.7)	−243.2085103/(−91.6)	−87.2
TS4″/4‴	−243.7870554/(−101.9)	−243.2186178/(−97.9)	−94.1
TS4″/P3	−243.7996863/(−109.8)	−243.2346387/(−108.0)	−104.2
TS4‴/9‴	−243.7719184/(−92.4)	−243.1999159/(−86.2)	−82.6
TS4‴/P3	−243.8012170/(−110.8)	−243.2348801/(−108.1)	−104.1
TS4‴/P8	−243.7945537/(−106.6)	−243.2141364/(−95.1)	−91.0
TS4‴/P13	−243.6813694/(−35.6)	−243.1175769/(−34.5)	−31.0
TS5/5′	−243.7909421/(−104.3)	−243.2231393/(−100.8)	−96.2
TS5/5‴	−243.7890270/(−103.1)	−243.2204179/(−99.1)	−95.1
TS5/12	−243.7622869/(−86.3)	−243.1946724/(−82.9)	−80.6
TS5/P2	−243.7987375/(−109.2)	−243.2279897/(−103.8)	−99.9
TS5/P4	−243.7731602/(−93.2)	−243.1997576/(−86.1)	−82.7
TS5′/5″	−243.7934854/(−105.9)	−243.2265283/(−102.9)	−98.3
TS5′/P2	−243.7952971/(−107.1)	−243.2277401/(−103.6)	−99.8
TS5′/P4	−243.7769724/(−95.6)	−243.2029626/(−88.1)	−84.6
TS5″/5‴	−243.7936896/(−106.0)	−243.2245608/(−101.7)	−97.5
TS5″/6	−243.7155463/(−57.0)	−243.1461015/(−52.4)	−42.0
TS5″/P2	−243.7913562/(−104.6)	−243.2224584/(−100.3)	−96.6
TS5″/P4	−243.8006954/(−110.4)	−243.2290080/(−104.4)	−100.5
TS5‴/15‴	−243.7340324/(−68.6)	−243.1633532/(−63.2)	−61.3
TS5‴/P2	−243.7412000/(−107.1)	−243.2248190/(−101.8)	−97.7
TS5‴/P4	−243.7972386/(−108.3)	−243.2258966/(−102.5)	−98.7
TS6/7	−243.8143904/(−119.0)	−243.2468645/(−115.6)	−112.5
TS6/P4	−243.8464347/(−139.1)	−243.2756350/(−133.7)	−129.6
TS6/P5	−243.8056788/(−113.6)	−243.2309812/(−105.7)	−101.3
TS7/7′	−243.8529007/(−143.2)	−243.2891608/(−142.2)	−137.0
TS7/P8	−243.8112658/(−117.1)	−243.2338512/(−107.5)	−103.5
TS7/P14	−243.7699317/(−91.1)	−243.2080221/(−91.3)	−86.9
TS7′/7′	−243.8065946/(−114.1)	−243.2431497/(−113.3)	−109.9
TS7′/P8	−243.7999958/(−110.0)	−243.2220387/(−100.1)	−96.9
TS7′/P14	−243.7763658/(−95.2)	−243.2117616/(−93.6)	−89.1
TS8/P3	−243.7996862/(−109.8)	−243.2346431/(−108.0)	−104.2
TS8/P8	−243.8009952/(−110.6)	−243.2207133/(−99.2)	−94.8
TS9/9′	−243.7788919/(−96.8)	−243.2043505/(−89.0)	−84.7
TS9/9‴	−243.7671241/(−89.4)	−243.1923520/(−81.4)	−77.0
TS9/P2	−243.7593580/(−84.5)	−243.1889320/(−79.3)	−76.9
TS9/P14	−243.7376035/(−70.9)	−243.1667258/(−65.4)	−61.6
TS9′/9″	−243.7697532/(−91.0)	−243.1943478/(−82.7)	−77.9
TS9′/10	−243.6495237/(−15.6)	−243.0777696/(−9.5)	−6.0
TS9′/11	−243.7430754/(−74.3)	−243.1730468/(−69.3)	−64.2
TS9′/P14	−243.7399136/(−72.3)	−243.1689703/(−66.8)	−62.8
TS9″/9‴	−243.7789787/(−96.8)	−243.2033495/(−88.3)	−83.2
TS9″/P14	−243.7485467/(−77.7)	−243.1784797/(−72.7)	−68.6
TS9‴/P12	−243.7659690/(−88.7)	−243.1949677/(−83.1)	−80.9
TS9‴/P14	−243.7514808/(−79.6)	−243.1824277/(−75.2)	−71.1

TABLE 3: (Continued)

species	B3LYP/6-311G**	CCSD(T)/6-311G**	CCSD(T)/6-311G**+ZPVE
TS10/10′	−243.6908993/(−41.5)	−243.1197075/(−35.8)	−31.6
TS10/14	−243.6496186/(−15.6)	−243.0782925/(−9.9)	−6.2
TS10/P9	−243.6850638/(−37.9)	−243.1074686/(−28.2)	−25.2
TS10/P13	−243.6543552/(−18.6)	−243.0868629/(−15.2)	−11.8
TS10′/14′	−243.6497515/(−15.7)	−243.0786975/ (−10.1)	−6.6
TS10′/10′	−243.6423425/(−11.1)	−243.0700169/(−4.7)	−2.2
TS11/11′	−243.7694053/(−90.8)	−243.2043469/(−89.0)	−83.7
TS11/11′*	−243.7237265/(−62.1)	−243.1534580/(−57.0)	−52.4
TS11/15	−243.7364315/(−70.1)	−243.1719674/(−68.6)	−64.3
TS11′/15′	−243.7393197/(−71.9)	−243.1753025/(−70.7)	−66.0
TS12/12′	−243.8198431/(−122.5)	−243.2557892/(−121.2)	−116.1
TS12/15′	−243.7039155/(−49.7)	−243.1386336/(−47.7)	−46.2
TS12/P1	−243.8033380/(−112.1)	−243.2300642/(−105.1)	−102.7
TS12′/15″	−243.7024587/(−48.8)	−243.1377139/(−47.2)	−45.6
TS12′/P1	−243.8041622/(−112.6)	−243.2303076/(−105.3)	−102.6
TS13/P5	−243.7164325/(−57.6)	−243.1382442/(−47.5)	−44.0
TS13/P11	−243.7345849/(−69.0)	−243.1573833/(−59.5)	−56.2
TS13′/13″	−243.7344684/(−68.9)	−243.1611232/(−61.8)	−57.6
TS13′/P5	−243.7253298/(−63.2)	−243.1482381/(−53.8)	−49.9
TS13′/P11	−243.7390627/(−71.8)	−243.1617691/(−62.2)	−58.7
TS13″/P5	−243.7412000/(−73.1)	−243.1652312/(−64.4)	−60.4
TS13″/P11	−243.7355104/(−69.5)	−243.1593913/(−60.8)	−57.4
TS13‴/P5	−243.7337400/(−68.4)	−243.1570267/(−59.3)	−55.7
TS13‴/P11	−243.7340286/(−68.6)	−243.1582776/(−60.1)	−57.3
TS14/14′	−243.6496433/(−15.7)	−243.0803403/(−11.2)	−7.4
TS14/P3	−243.6469527/(−14.0)	−243.0800456/(−11.0)	−7.1
TS14′/P3	−243.6470078/(−14.0)	−243.0799792/(−10.9)	−7.4
TS15/15′	−243.7348326/(−69.1)	−243.1704474/(−67.7)	−64.4
TS15/15‴	−243.7430859/(−74.3)	−243.1801293/(−73.8)	−69.5
TS15′/15″	−243.7439735/(−74.8)	−243.1813921/(−74.6)	−69.8
TS15″/15‴	−243.7319640/(−67.3)	−243.1676462/(−65.9)	−62.8
TS16/P11	−243.7055037/(−50.7)	−243.1298680/(−42.2)	−41.0
TSP1/P1	−243.8133424/(−118.4)	−243.2560996/(−121.4)	−119.8
TSP2/P2	−243.8397455/(−134.9)	−243.2810604/(−137.1)	−134.7
TSP5/P8	−243.8096790/(−116.1)	−243.2306337/(−105.5)	−104.3
TSP6/P7	−243.6706716/(−28.9)	−243.0925521/(−18.1)	−14.9

14′ (−6.6), and **TS9′/10** (−6.0) are considerably higher in energy than **TS10/P$_{13}$** (−11.8) and **TS10/P$_9$** (−25.2). Then, paths **P$_3$** and **P$_2$**, **P$_{12}$**, **P$_{14}$** are much less competitive than path **P$_9$** and even path **P$_{13}$**. Note that the values in parentheses are relative energies with reference to **R**.

Path **P$_1$** is associated with the O-shift of **1** to the very low lying branched isomer OC(H)NO (**2**) followed by easy conversion to **2′**. Both **2** and **2′** can dissociate to **P$_1$** (HCO + NO) via the direct C−N rupture. Since the O-shift transition state **TS1/2** (−7.3) is energetically much higher than **TS1/P$_6$** (−19.4) and **TS1/10** (−13.5), path **P$_1$** cannot compete with paths **P$_6$** and **P$_9$**. Yet, the competition between **P$_1$** and **P$_{13}$** is somewhat difficult to predict without dynamical calculations since the reverse conversion from **2** to **1** is unfeasible due to the rather large exothermicity of **2** (−132.3 kcal/mol) whereas the conversion from **10** to **1** is much more likely.

It is worthy of mentioning that the large heat (−132.3 kcal/mol) released from the reactant **R** to the low-lying intermediate OC(H)NO (**2**) may make many conversion pathways possible leading to various products including the lowest-energy **P$_4$** (^{3}NH + CO_2), as shown in Figure 5b,c. However, the initial transition states such as **TS2/4** (−79.7), **TS2/9′** (−60.9), and **TS2′/3** (−63.5) are much higher in energy than **P$_1$** (HCO + NO). As a result, starting from **2**, formation of the other products is much less likely than that of **P$_1$**. Then, the details of Figure 5b,c are not discussed here. It should be pointed out that the whole complex triplet potential energy surface might be useful for future discussion on the other reactions such as HNCO with ^{3}O.

3.3. Reaction Mechanism via the Triplet PES and Experimental Implications. From sections 3.1 and 3.2, we know that on the triplet PES of the CH + NO_2 reaction, the CH and NO_2 radicals can indeed be brought together barrierlessly via the initial top-N attack to form the isomer $HCNO_2$ (**1**). Subsequently, the most feasible pathway is the direct O-extrusion of **1** to give **P$_6$** (HCNO + ^{3}O). Much less competitively **1** can isomerize to the species HON(O)C (**10**) that can easily dissociate to **P$_9$** (CNO + OH). The products **P$_{13}$** (HONC + ^{3}O) and **P$_1$** (HCO + NO) may have even smaller yields. Formation of many other products seems unlikely due to kinetic factors, although they are thermodynamically much more favored than **P$_6$** and **P$_9$**.

It may be of interest to make a rough comparison between the triplet and singlet PESs of the CH + NO_2 reaction. On the singlet PES calculated by Tao et al. very recently,[4] $HCNO_2$ is also barrierlessly formed as the initial adduct (the nature is slightly different; i.e., triplet $HCNO_2$ is of top-N attack while singlet $HCNO_2$ is of side N−O attack). With reference to the reactant, the relative energies of singlet and triplet $HCNO_2$ are −57.3 and −50.6 kcal/mol, respectively, indicating that the singlet species is thermodynamically more favored. A striking difference is that singlet $HCNO_2$ can almost barrierlessly lead to the very low lying singlet OC(H)NO with just 0.2 kcal/mol, whereas triplet $HCNO_2$ is stabilized by a considerable barrier of at least 31.2 kcal/mol (for **1** → **P$_6$** conversion). As a result, on the singlet PES, **P$_1$** (HCO + NO) may be the most feasible primary product that may further dissociate to the final secondary product **P$_{12}$** (H + CO + NO) (^{1}HNO + CO and ^{1}HON +

TABLE 4: Harmonic Vibration Frequencies (cm^{-1}) with Infrared Intensities in Parentheses (km/mol) for Triplet $CHNO_2$ Isomers at the B3LYP/6-311G(d,p) Level

isomer	harmonic frequencies and infrared intensities
1	395(12), 492(8), 674(9), 711(15), 980(23), 1048(22), 1291(107), 1491(170), 3180(10)
2	222(9), 369(7), 590(13), 912(145), 951(0), 134930), 1640(27), 1768(287), 2983(27)
2'	305(3), 353(11), 710(12), 898(200), 958(1), 1367(5), 1661(7), 1727(202), 3078(34)
3	299(5), 433(6), 584(72), 804(50), 900(8), 1286(7), 1489(48), 1877(157), 3458(9)
3'	245(3), 364(24), 607(0), 674(86), 1041(53), 1351(6), 1466(3), 1852(210), 3315(0)
4	247(5), 369(22), 614(1), 653(97), 876(69), 1176(49), 1381(65), 1850(135), 3510(26)
4'	222(1), 379(1), 604(111), 606(3), 887(27), 1160(116), 1409(118), 1843(97), 3758(138)
4''	240(8), 285(2), 631(105), 782(44), 871(33), 1035(62), 1327(66), 1814(111), 3753(127)
4'''	326(21), 339(64), 691(84), 825(10), 872(63), 1090(42), 1412(88), 1782(128), 3511(18)
5	218(9), 335 (10), 486(64), 594(0), 928(243), 1022(40), 1476(43), 1902(208), 3281(6)
5'	214(0), 353(3), 488(85), 600(1), 936(181), 1051(50), 1492(107), 1908(216), 3366(1)
5''	291(1), 304(31), 513(63), 757(2), 853(55), 967(130), 1467(41), 1888(269), 3361(1)
5'''	320(15), 329(81), 503(19), 796(5), 837(61), 937(88), 1460(60), 1866(245), 3290(1)
6	346(3), 377(35), 556(8), 624(11), 746(45), 999(181), 1181(23), 1780(225), 3376(14)
7	414(26), 482(146), 577(7), 672(22), 914(27), 1144(4), 1318(358), 1671(129), 3773(84)
7'	434(3), 530(61), 569(43), 708(94), 917(1), 1155(269), 1375(35), 1675(229), 3753(91)
8	240(8), 286(2), 632(105), 782(44), 874(33), 1034(62), 1377(66), 1813(110), 3752(127)
9	277(0), 378(42), 630(6), 690(122), 908(1), 1242(108), 1333(252), 1574(74), 3570(28)
9'	276(0), 380(12), 626(4), 646(95), 954(23), 1267(436), 1332(47), 1589(62), 3814(221)
9''	210(22), 433(35), 526(31), 655(71), 919(32), 1213(357), 1258(4), 1474(102), 3800(166)
9'''	198(43), 431(111), 448(34), 655(60), 899(36), 1200(191), 1278(159), 1462(67), 3589(37)
10	393(134), 454(21), 511(5), 578(4), 776(145), 1117(21), 1246(136), 1437(59), 3702(76)
10'	356(93), 472(1), 509(39), 568(8), 803(175), 1117(121), 1238(32), 1457(28), 3699(87)
11	269(128), 446(9), 548(10), 823(29), 939(11), 1108(53), 1220(255), 1458(113), 3804(101)
11'	297(131), 449(7), 542(4), 829(32), 936(29), 1097(19), 1229(266), 1443(104), 3825(120)
12	171(13), 353(14), 593(11), 936(319), 1003(0), 1140(129), 1378(0), 1882(332), 3058(23)
12'	286(2), 287(15), 736(12), 911(247), 990(0), 1078(168), 1383(4), 1858(276), 3086(26)
13	153(6), 299(2), 515(55), 666(97), 764(153), 776(155), 1118(13), 1907(113), 3462(34)
13'	173(5), 333(12), 587(9), 688(83), 802(217), 1051(14), 1154(52), 1773(73), 3560(76)
13''	298(1), 338(19), 683(84), 690(125), 766(19), 923(48), 1074(65), 1776(104), 3561(74)
13'''	287(11), 308(15), 659(67), 676(54), 677(14), 840(198), 988(12), 1904(126), 3451(35)
14	261(21), 313(99), 493(36), 552(30), 811(136), 875(27), 1232(134), 1146(34), 3757(121)
14'	208(84), 259(70), 485(51), 536(24), 828(145), 904(51), 1243(39), 1379(58), 3688(77)
15	210(2), 336(3), 599(14), 774(127), 872(166), 1105(301), 1311(232), 1368(24), 3521(14)
15'	216(0), 337(3), 606(5), 714(94), 956(324), 1125(189), 1306(57), 1344(207), 3817(187)
15''	294(1), 320(3), 719(12), 727(96), 927(236), 971(50), 1268(127), 1324(159), 3813(178)
15'''	226(36), 333(9), 631(134), 702(84), 733(116), 1063(34), 1275(284), 1352(46), 3524(39)
16	184(12), 190(8), 297(52), 390(3), 737(103), 1218(53), 1473(79), 2138(9), 3161(78)

CO may also have certain contributions to $\mathbf{P_{12}}$). However, $\mathbf{P_6}$ (HCNO + ^{3}O) and $\mathbf{P_9}$ (CNO + OH) may be the first and second feasible products on the triplet PES. Moreover, $\mathbf{P_6}$ and $\mathbf{P_9}$ may not take secondary dissociation such as to $\mathbf{P_{16}}$ (H + CNO + ^{3}O) or $\mathbf{P_{18}}$ (^{3}O + OH + CN) due to the energetic hindrance, as shown in Table 1.

The triplet PES of the reaction CH + NO_2 is quite similar to that of another simple yet very important reaction CH + NO. For the latter reaction, the major pathway is formation of an initial N-attack isomer HCNO that can easily dissociate to HCN + ^{3}O.[6] It should be pointed out that the conversion from the triplet $HCNO_2$ to the singlet OC(H)NO via an intersystem crossing transition state with much lower energy than triplet **TS1/2** seems unlikely since the singlet transition state between singlet $HCNO_2$ and OC(H)NO is already 6.5 kcal/mol lower than triplet $HCNO_2$.

It seems reasonable for us to assume similar entering probability for the addition reaction between CH and NO_2 radicals to form either singlet or triplet $HCNO_2$ via attractive potentials. Then, the room-temperature rate constants for formation of the triplet adduct $HCNO_2$ may also be fast as for the singlet $HCNO_2$. To gain a deep understanding of the CH + NO_2 reaction mechanism, simple RRKM calculations[9] are performed on the basis of both the triplet PES in the present work and the singlet PES by Tao et al.[4] We consider the following reaction pathways:

$$\mathbf{R}\ (CH + NO_2) \rightleftharpoons \mathbf{1}\ HCNO_2^* \rightarrow \mathbf{P_6}\ (HCNO + {}^3O)$$
$$\rightleftharpoons \mathbf{10}\ (HON(O)C^*) \rightarrow \mathbf{P_9}\ (CNO + OH)$$
$$\rightarrow \mathbf{P_{13}}\ (HONC + {}^3O)$$
$$\rightleftharpoons \mathbf{2}\ (cos\text{-}OC(H)NO^*) \rightleftharpoons \mathbf{2'}\ (trans\text{-}OC(H)NO^*) \rightarrow \mathbf{P_1}\ (HCO + NO)$$
$$\rightarrow \mathbf{P_1}\ (HCO + NO)$$

for the triplet PES and

$$\mathbf{R}\ (CH + NO_2) \rightleftharpoons \mathbf{1}\ (HCNO_2^*) \rightarrow \mathbf{2}\ (cis\text{-}OC(H)NO)\ [\mathbf{P_1}\ (HCO + NO)]$$

for the singlet PES, respectively. The symbol "*" represents the vibrational excitation of the intermediates. Note that on the singlet PES, the reverse conversion from **2** to **1** and the dissociation of **2** to $\mathbf{P_1}$ are not considered since **2** is rather energetic (−140.2 kcal/mol relative to **R**) and its dissociation to $\mathbf{P_1}$ is very easy.

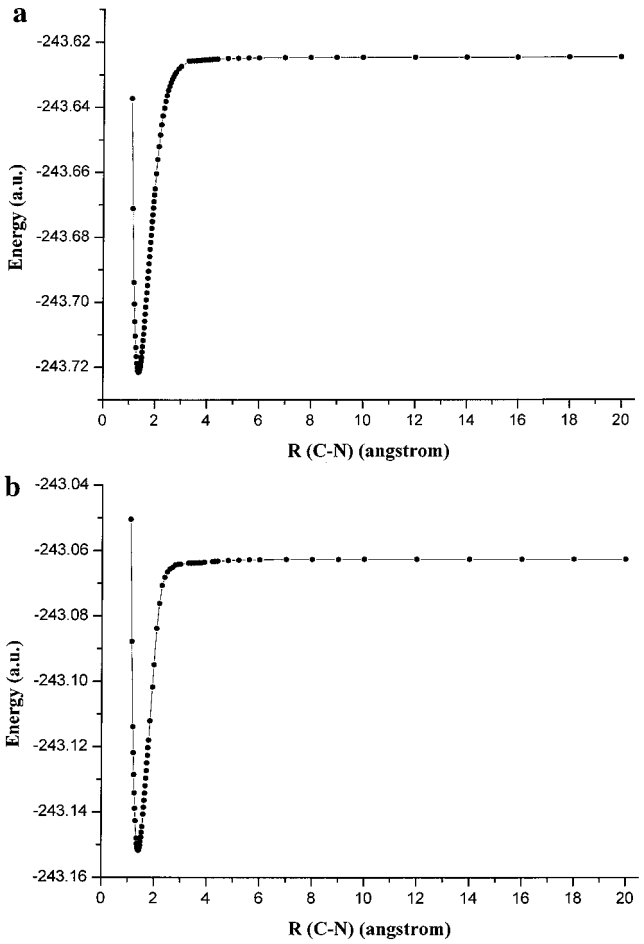

Figure 4. (a) Potential curves of the initial N-attack of the CH radical to NO_2 at the B3LYP/6-311G(d) level. (b) Potential curves of the initial N-attack of the CH radical to NO_2 at the CCSD(T)/6-311G(d,p)//B3LYP/6-311G(d,p) level. The calculations are performed by pointwise optimization of the remaining varied bond lengths or bond angles with every fixed internal C−N bond length. During the optimization, the symmetry is constrained as C_s.

Under the condition of 298 K and 2 Torr, the total rate constant for the CH + NO_2 via the singlet PES is calculated to be 1.45×10^{-10} cm^3 $molecule^{-1}$ s^{-1}, very close to the experimental value 1.67×10^{-10} cm^3 $molecule^{-1}$ s^{-1}. Via the triplet PES, the theoretical value is 5.14×10^{-12} cm^3 $molecule^{-1}$ s^{-1}, much slower than that via the singlet PES. The branching ratios of the most favorable dissociation products **P1** (HCO + NO), **P6** (HCNO + ^{3}O), **P9** (CNO + OH), **P13** (HONC + ^{3}O) and stabilization of isomer **1** on the triplet PES are calculated with reference to 298 K and different pressures, as plotted in Figure 6. It is found that under the pressure of less than 10^5 Torr, the branching ratios of various species keep constant, i.e., **P6** (87%), **P9** (8.9%), **P1** (3.2%), **P13** (1%), and **1** (0%). Then the stabilization of isomer **1** can be neglected compared to its dissociation. When the pressure is larger than 10^5 Torr, the stabilization branching ratio of **1** starts to increase dramatically along with the decrease of its dissociation branching ratios (the decrease of **P6** branching ratio is great). Only when the pressure reaches 10^7 Torr can stabilization dominate over dissociation for isomer **1**. Then, for the title reaction via the triplet PES, the pressure effect is unimportant over a wide range of pressure despite that isomer **1** is stabilized by 31.2 kcal/mol.

There has been only one experimental investigation on the product distributions of the CH + NO_2 reaction by Rim and Hershberger recently.[3] They found the major product channel to be H + CO + NO or HNO + CO (together account for 92 ± 4%) and the minor to be HCO + NO (accounting for 8 ± 4%). Surely, the singlet PES by Tao et al.[4] can well interpret the CO formation of the title reaction, and the present RRKM rate constant is in close agreement with the measured value.[3] Rim and Hershberger[3] found HCNO to have undetectably low yield and they claimed that "what is somewhat surprising is that dissociation of the $HCNO_2$ complex to form O + HCNO is not observed". Since the estimated total rate constant via the triplet PES by simple RRKM calculations, though still fast, is significantly smaller than that via the singlet PES, we suggest that the triplet PES may be less important than the singlet PES for the CH + NO_2 reaction. However, it is worthy of pointing out that the main products **P6** (HCNO + ^{3}O) and **P9** (CNO + OH) of the triplet PES contain very reactive and important radicals ^{3}O, CNO, and OH that may further initiate many reactions in combustion chains and that, most importantly, no nitrogen oxides are emitted on triplet PES, indicative of the very effective reduction of NO_2 by the CH radical. On the singlet PES, NO is produced exclusively for the CH + NO_2 reaction. Therefore, due to the distinct discrepancies between the present triplet PES study and Tao et al.'s singlet PES[4] and Rim and Hershberger's experimental investigations,[3] further experimental studies are still desirable to detect HCNO, CNO, and OH in order to clarify the reaction mechanism of CH + NO_2.

It should be pointed out that even on the triplet PES, the low-lying products **P4** ^{3}NH + CO_2 (−161.1) and **P5** HNCO + ^{3}O (−120.4) still seem unlikely to be formed for the CH + NO_2 reaction. As shown in Figure 5,c, their formation cannot kinetically compete with that of **P1** (HCO + NO) (−119.7) although **P1** is also quite unfeasible compared to **P6** (HCNO + ^{3}O) and **P9** (CNO + OH).

4. Conclusions

A detailed triplet potential energy surface of the CH + NO_2 reaction system is built up at the B3LYP and CCSD(T) (single-point) levels. We find that the initial step is a barrierless top-N attack of the CH radical at NO_2 to form the triplet isomer $HCNO_2$ (**1**). Subsequently, the direct O-extrusion of **1** gives **P6** (HCNO + ^{3}O). Much less competitively **1** may take a 1,3-H shift conversion to the branched isomer HON(O)C (**10**) that can directly dissociate to product **P9** (CNO + OH). Since the involved intermediate isomers and transition states in the above channels are all energetically lower than the reactant **R**, the title reaction may proceed fast around room temperature via the triplet PES, as confirmed by the RRKM calculations. Our calculations indicate that the triplet PES may have some contribution in the CH + NO_2 combustion chemistry. However, the mechanism of the CH + NO_2 reaction via the triplet PES is quite different from that via the singlet PES calculated by Tao et al. and from the experimental observation by Rim and Hershberger. We suggest that future experimental investigations on this important radical reaction be desirable with a focus on determining the products **P6** (HCNO + ^{3}O) and **P9** (CNO + OH).

Acknowledgment. This work is supported by the National Natural Science Foundation of China (No. 29892168, No. 20073014), Doctor Foundation by the Ministry of Education, Foundation for University Key Teacher by the Ministry of Education, and Key Subject of Science and Technology by the Ministry of Education of China. We are greatly thankful for the referees' helpful comments.

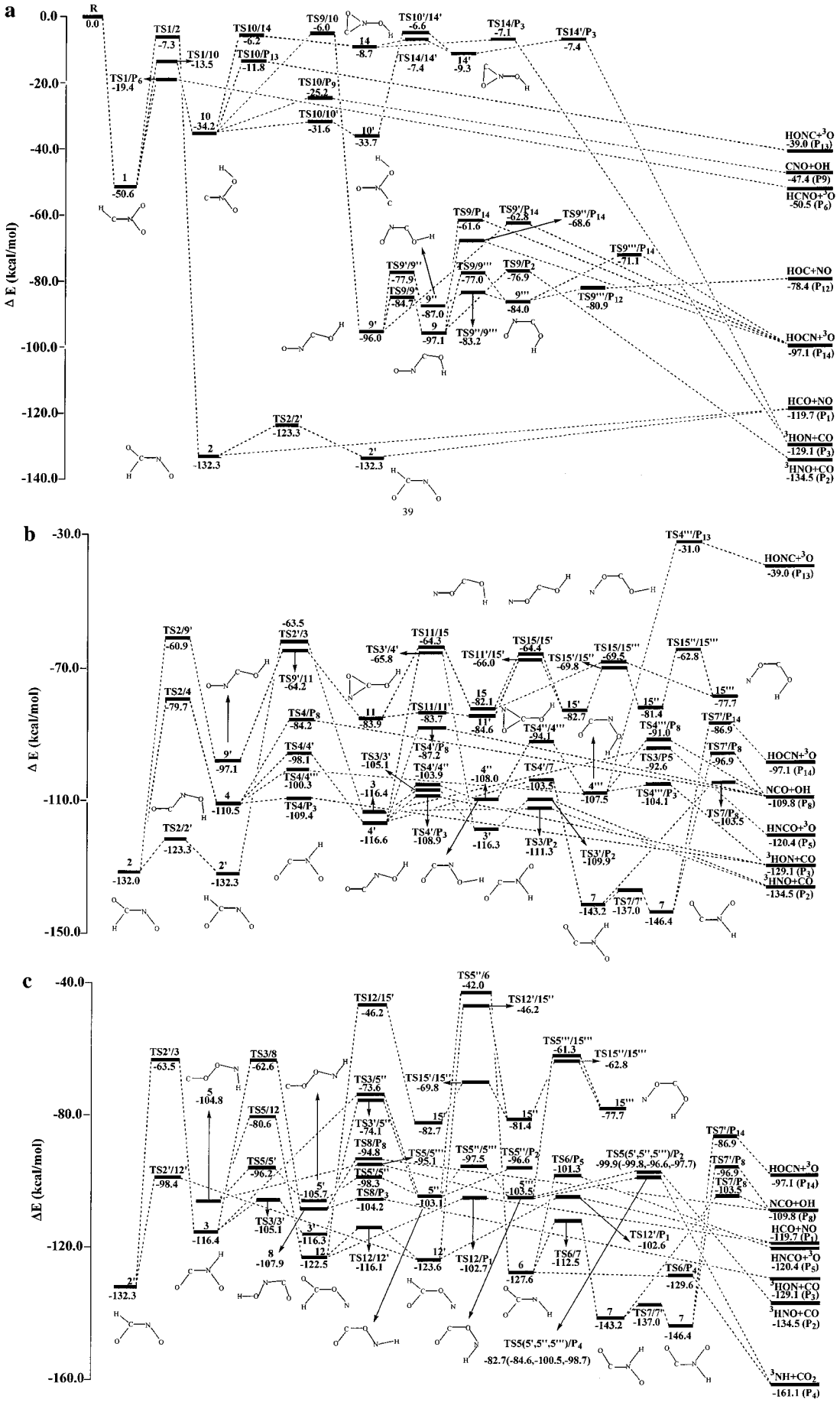

Figure 5. Schematic pathways for the CH + NO_2 reaction at triplet PES. Relative energies are calculated at the CCSD(T)/6-311G(d,p)//B3LYP/6-311G(d,p)+ZPVE level.

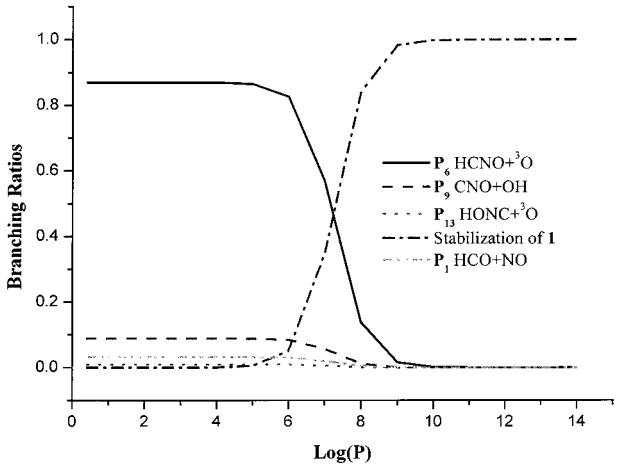

Figure 6. Branching ratios for dissociation of isomer **1** ($HCNO_2$) to $\mathbf{P_1}$ (HCO + NO), $\mathbf{P_6}$ (HCNO + ^{3}O), $\mathbf{P_9}$ (CNO + OH), $\mathbf{P_{13}}$ (HONC + ^{3}O) and stabilization of isomer **1** at 298 K and different pressures (in Torr).

References and Notes

(1) (a) Miller, J. A.; Bowman, C. T. *Prog. Energy Combus. Sci.* **1989**, *15*, 287. (b) Strobel, D. F. *Planet Space Sci.*, **1982**, *30*, 839.

(2) Wagal, S. S.; Carrington, T.; Filseth, S. V.; Sadowski, C. M. *Chem. Phys.* **1982**, *69*, 61.

(3) Rim, K. T.; Hershberger, J. F. *J. Phys. Chem. A* **1998**, *102*, 4592.

(4) Tao, Y. G.; Ding, Y. H.; Li, Z. S.; Huang, X. R.; Sun, C. C. *J. Phys. Chem. A* **2001**, *105*, 3388.

(5) (a) Bocherel, P.; Herbert, L. B.; Rowe, B. R.; Sims, I. R.; Smith, I. W. M.; Travers, D. *J. Phys. Chem.* **1996**, *100*, 3063. (b) Jursic, B. S. *J. Phys. Chem. A* **1998**, *102*, 9225. (c) Dean, A. M.; Hanson, R. K.; Bowman, C. T. *J. Phys. Chem.* **1991**, *95*, 3180. (d) Lambrecht, R. K.; Hershberger, J. F. *J. Phys. Chem.* **1994**, *98*, 8406. (e) Mebel, A. M.; Luna, A. M.; Lin, C.; Morokuma, K. *J. Chem. Phys.* **1996**, *105*, 6439. (f) Bergeaut, A.; Calvo, T.; Daugey, N.; Loison, J. C.; Dorthe, G. *J. Phys. Chem. A* **1998**, *102*, 8124. (g) Jursic, B. S. *J. Phys. Chem. A* **1999**, *103*, 1880.

(6) (a) Marchard, N.; Jimeno, P.; Rayez, J. C.; Liotard, D. *J. Phys. Chem. A* **1997**, *101*, 6077. (b) Marchard, N.; Rayez, J. C.; Smith, S. C. *J. Phys. Chem. A* **1998**, *102*, 3358.

(7) Geiger, H.; Wiesen, P.; Becker, K. H. *Phys. Chem. Chem. Phys.* **1999**, *1*, 5601 and reference therein.

(8) Frisch, M. J.; Trucks, G. W.; Schlegel, H. B.; Scuseria, G. E.; Robb, M. A.; Cheeseman, J. R.; Zakrzewski, V. G.; Montgomery, J. A., Jr.; Stratmann, R. E.; Burant, J. C.; Dapprich, S.; Millam, J. M.; Daniels, A. D.; Kudin, K. N.; Strain, M. C.; Farkas, O.; Tomasi, J.; Barone, V.; Cossi, M.; Cammi, R.; Mennucci, B.; Pomelli, C.; Adamo, C.; Clifford, S.; Ochterski, J.; Petersson, G. A.; Ayala, P. Y.; Cui, Q.; Morokuma, K.; Malick, D. K.; Rabuck, A. D.; Raghavachari, K.; Foresman, J. B.; Cioslowski, J.; Ortiz, J. V.; Stefanov, B. B.; Liu, G.; Liashenko, A.; Piskorz, P.; Komaromi, I.; Gomperts, R.; Martin, R. L.; Fox, D. J.; Keith, T.; Al-Laham, M. A.; Peng, C. Y.; Nanayakkara, A.; Gonzalez, C.; Challacombe, M.; Gill, P. M. W.; Johnson, B. G.; Chen, W.; Wong, M. W.; Andres, J. L.; Head-Gordon, M.; Replogle, E. S.; Pople, J. A. *Gaussian 98*, revision A7; Gaussian, Inc.: Pittsburgh, PA, 1998.

(9) (a) Diau, E. W. G.; Lin, M. C.; Melius, C. F. *J. Chem. Phys.* **1994**, *101*, 3923. (b) Berman, M. R.; Lin, M. C. *J. Chem. Phys.* **1983**, *87*, 3933.